

CO₂ capture using boron, nitrogen, and phosphorus-doped C₂₀ in the present electric field: A DFT study

Parham Rezaee,^{*,†,‡} Shervin Alikhah Asl,[¶] Mohammad Hasan Javadi,[§] Shahab Rezaee,[‡] Razieh Morad,[†] Mahmood Akbari,^{*,†} Seyed Shahriar Arab,[‡] and Malik Maaza[†]

[†]*UNESCO-UNISA Africa Chair in Nanoscience and Nanotechnology (U2ACN2), College of Graduate Studies, University of South Africa (UNISA), Pretoria, South Africa*

[‡]*Department of Biophysics, School of Biological Sciences, Tarbiat Modares University, Tehran, Iran*

[¶]*Unit 12, 3rd Floor, Sahel Apartment, Motahhari St., Ardabil, Iran*

[§]*Unit 1, NO. 17, Keyhan 2 Aly., Keyhan St., Ayatollah Kashani boulevard, Tehran, Iran*

E-mail: parham.rezaee@modares.ac.ir; makbari@tlabs.ac.za

Abstract

Burning fossil fuels emits a significant amount of CO₂, causing climate change concerns. CO₂ Capture and Storage (CCS) aims to reduce emissions, with fullerenes showing promise as CO₂ adsorbents. Recent research focuses on modifying fullerenes using an electric field. In light of this, we carried out DFT studies on some B, N, and P doped C₂₀ C_{20-n}X_n (n = 0, 1, 2, and 3; X = B, N, and P) in the absence and presence of an electric field in the range of 0-0.02 *a.u.*. The cohesive energy was calculated to ensure their thermodynamic stability showing, that despite having lesser cohesive energies than C₂₀, they appear in a favorable range. Moreover, the charge distribution for all structures was depicted using the ESP map. Most importantly, we evaluated the adsorption energy, height, and CO₂ angle, demonstrating the B and N-doped fullerenes had the stronger interaction with CO₂, which by far exceeded C₂₀'s, improving its physisorption to physicochemical adsorption. Although the adsorption energy of P-doped fullerenes was not as satisfactory, in most cases, increasing the electric field led to enhancing CO₂ adsorption and incorporating chemical attributes to CO₂-fullerene interaction. The HOMO-LUMO plots were obtained by which we discovered that unlike the P-doped C₂₀, the surprising activity of B and N-doped C₂₀s against CO₂ originates from a high concentration of the HOMO-LUMO orbitals on B and N atoms. Additionally, the charge distribution for all structures was depicted using the ESP map. In the present article, we attempt to introduce more effective fullerene-based materials for CO₂ capture as well as strategies to enhance their efficiency and revealing adsorption nature over B, N, and P-doped fullerenes.

Introduction

The persistent reliance on burning fossil fuels to produce energy has significantly escalated the levels of CO_2 in the atmosphere over the past century. Although there have been many concerns about global climate changes and numerous efforts to develop sustainable energy sources, the combustion of fossil fuels remains the primary method of generating electricity, leading to the release of 13 Gt of CO_2 into the atmosphere annually. Consequently, CO_2 Capture and Storage (CCS) technology emerges as a promising approach to mitigate CO_2 emissions. While solvent absorption using amines is the conventional method for capturing CO_2 , it faces criticism due to its high energy consumption and operational limitations such as corrosion, slow uptake rates, foaming, and size-able equipment. Thus, there is a significant tendency to explore solid adsorbent materials for CCS purposes. In recent years, metal-organic frameworks (MOFs) have gained attention as solid CO_2 adsorbents thanks to their adjustable chemical and physical properties. Notably, research into metal-free carbon-based nanomaterials for gas adsorption is rapidly increasing.¹⁻¹⁰

Fullerene molecules are a unique type of hollow spheres consisting entirely of carbon atoms, with various numbers of carbon atom. These molecules are intriguing for use in diverse electrochemical and adsorption applications because of their low reduction potential and high electron acceptivity.¹¹

Scientists have conducted a wide range of experimental and theoretical studies to examine how modifications to the fullerene cage can affect its chemical reactivity and properties, making it a promising source of new materials for organometallic systems or as adsorbents. Fullerenes, along with other carbon-based nanomaterials such as carbon nanotubes and graphene, offer excellent stability for the capture of carbon dioxide.^{12,13}

Dry adsorption, which uses adsorbents such as activated carbons or molecular sieves, is an effective method for absorbing CO_2 . Although metal-organic frameworks (MOFs) have gained popularity as a solid CO_2 adsorbent,

researchers are still interested in investigating metal-free carbon-based or nitrogen-rich materials for gas adsorption.¹⁴⁻¹⁷

Nitrogen-rich materials are effective at capturing CO_2 due to the presence of N lone pairs. Amine scrubbing, a separation technique that has been utilized since the 1930s, is a reliable method for separating CO_2 from natural gas and hydrogen, both in dry and wet forms. In previous research, we have demonstrated the effectiveness of various anions and N-rich molecular systems, such as guanidine and its cyclic and acyclic derivatives, in capturing CO_2 . The lone pair of electrons on the imine N serves as the attachment point for CO_2 capture, resulting in covalently bonded zwitterion clusters formed by the electron donation from the imine N to the C of CO_2 .¹⁸⁻²¹

Recently, porous carbon nanostructures doped with nitrogen have become popular due to their excellent adsorption properties, low-cost synthesis, and larger surface area. Reactive magnetron sputtering or chemical vapor deposition are methods used to synthesize these structures. The insertion of N atom into carbon structures activates the carbon π -electrons, making the N-C polarized bonds preferred sites for electrophilic/nucleophilic attack. Researchers have proposed a novel porous fullerene, $\text{C}_{24}\text{N}_{24}$, consisting of eight s-triazine rings with six N_4 cavities similar to porphyrin. Transition metal and porous Si or Fe doped $\text{C}_{24}\text{N}_{24}$ fullerenes have exhibited efficient hydrogen storage and catalytic activity for CO oxidation and NO reduction. The N_4 cavities in the $\text{C}_{24}\text{N}_{24}$ fullerene are preferred sites for anchoring metals due to the formation of strong N-metal covalent bonds without host metal aggregation.²²⁻²⁵

Furthermore, researchers have proposed applying an electric field to control the capture of CO_2 . Studies show that an electric field of 0.05 a.u. enhanced the adsorption energy of carbon dioxide from 2.4 to 19.3 kcal/mol. The material was recovered by a spontaneous exothermic reaction of 75.1 kcal/mol when the field was turned off. Similarly, the mechanism of CO_2 adsorption changed from physisorption to chemisorption after applying the electric

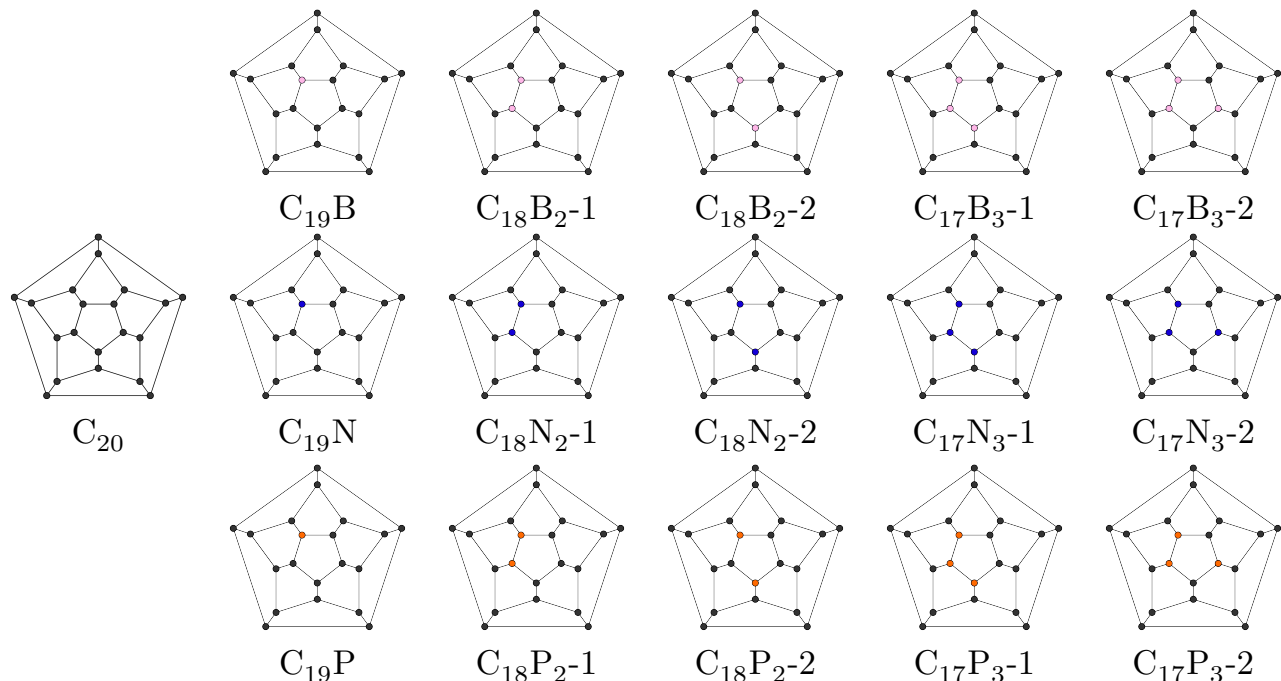


Figure 1: The schlegel diagram indicating the position of X atoms in X-doped fullerene systems. ($C_{20-n}X_n$ ($n = 0, 1, 2,$ and 3 ; $X = B, N,$ and P))

field, and by turning off the electric field, CO_2 was desorbed from the adsorbent. C_3N , penta graphene, and P-doped graphene also demonstrated a good adsorption affinity for CO_2 in the presence of an electric field. In recent studies, it was found that P-doped C_{60} fullerene is an excellent selective adsorbent for CO_2 in the presence of an electric field of 0.014 a.u.²⁶⁻³⁰

In this study, DFT method have been employed to determine the stability and CO_2 adsorption activity of some doped C_{20} fullerenes. These fullerenes include B, N, and P-doped C_{20} with the various numbers of the doped atoms consisting of $C_{19}X$, $C_{18}X_2$, and $C_{17}X_3$ ($X = B, N,$ and P) and also, with different geometry in which the atoms are side by side displayed by $C_{18}X_2-1$ and $C_{17}X_3-1$ or with a carbon atom separating them as $C_{18}X_2-2$ or two next to each other and one apart with a carbon atom between, from each side in a pentagon as $C_{17}X_3-2$. Fig. 1 depicts the schlegel diagram of different structures in which X atoms are positioned. Cohesive Energy (CE) for the doped C_{20} s have been calculated as an indicator of thermodynamic stability in various electric fields (EF). In order to evaluate the candidate doped fullerene's tendency to capture CO_2 and

electric field's effect, adsorption energy (AE), height (AH), and CO_2 angle have been computed in the different EFs. Apart from the HOMO-LUMO plots and analysis, the electrostatic potential surface maps (ESP maps) were also obtained, to demonstrate the charge distribution of doped fullerenes and their potential as a CO_2 capture agents.

Computational details

All calculations have been carried out at the B3LYP/6-311++G(d,p) level of the spin unrestricted density functional theory using the Gaussian 09 suite of programs. The vibrational frequency analysis has been done to confirm the optimized geometries as the energy minima. The DFT-D3 (Grimme's scheme) empirical correction was applied for the van der Waals interactions. The geometrical optimizations were performed at convergence-tolerance of 5×10^{-7} Ha for the energy, $4.5 \times 10^{-4} E_h \text{ \AA}^{-1}$ for the force and $1.8 \times 10^{-3} \text{ \AA}$ for the displacement. In addition, the ESP maps were plotted for all fullerenes in the absence of EF to illustrate the charge distribution with isovalue $0.004 e\text{ \AA}^{-3}$.

Table 1: The amounts of cohesive energy (eV) for $C_{20-n}X_n$ ($n = 1, 2, \text{ and } 3$; $X = \text{B, N, and P}$)

	X=B	X=N	X=P
$C_{19}X$	7.780	7.805	7.685
$C_{18}X_2-1$	7.652	7.720	7.550
$C_{18}X_2-2$	7.684	7.727	7.615
$C_{17}X_3-1$	7.460	7.619	7.476
$C_{17}X_3-2$	7.479	7.617	

Also, the HOMO – LUMO orbitals were shown for fullerenes in the aforementioned situation.

The cohesive energy representing the energy required to decompose the fullerene into isolated atoms is defined as:

$$E_{coh} = \frac{\sum n_x E_x - E_T}{\sum n_x} \quad (1)$$

where n_x is the number of atom x in the fullerene structure, E_x and E_T denote the isolated atom x and the total energies of the fullerene, respectively.

The adsorption energy (E_{ads}) of each adsorbate was obtained by:

$$E_{ads} = E_{fullerene+CO_2} - (E_{fullerene} + E_{CO_2}) \quad (2)$$

where $E_{fullerene+CO_2}$, $E_{fullerene}$ and E_{CO_2} are the total energies of the fullerene and CO_2 complex, the fullerene, and CO_2 molecule, respectively. The adsorption height was calculated according to the minimum distance of the fullerenes and CO_2 atoms.

Results and discussion

Geometrical configuration and stability of doped fullerene

Prior to investigating the adsorption of CO_2 molecules over doped fullerene, the optimized geometry of the free gas molecule was computed. The findings reveal that the bond length of the C–O is 1.178 Å, and the O–C–O angle is 180° in CO_2 . Our structural parameter calculations closely align with previous experimental

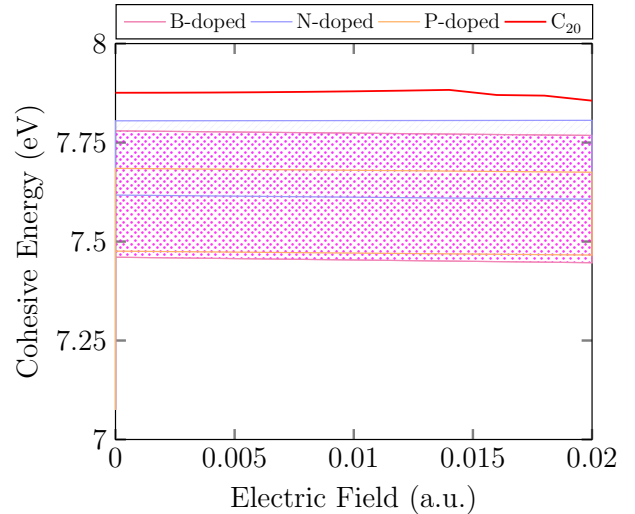


Figure 2: Variation of cohesive energy for C_{20} , B, N, and P-doped C_{20} in 0–0.02 *a.u.* electric field.

results. Molecular orbital calculations of CO_2 gas molecules indicate that the HOMO orbital (the highest occupied molecular orbitals) of the CO_2 molecule mainly comprises $O(2p)$ orbitals perpendicular to the axial direction of CO_2 , housing the lone pair electrons. The LUMO orbital (the lowest unoccupied molecular orbitals) primarily consists of anti- σ bonds of $C(2s)$ and $O(2p)$, which are parallel to the CO_2 's axial direction. The energy levels of HOMO and LUMO are -10.50 eV and -0.53 eV, in order. Since the energy well for the HOMO of CO_2 is too low, it is unable to sufficiently overlap with the conduction band of any material while the energy well for the LUMO of CO_2 is high enough to readily overlap with the valence band of suitable materials, aiding adsorption process.

The geometry of doped fullerenes are optimized except $C_{17}P_3-2$ fullerene, which was completely unstable. According to the equation 1, table 1 demonstrates that the cohesive energy (CE) for all doped fullerenes are thermodynamically stable. This also shows that incorporation of the X atoms into fullerenes is energetically possible. Fig. 2 shows an overview of B, N, and P-doped fullerenes' (C_{20}) CE (eV) in the range of 0 – 2×10^{-2} *a.u.* EF. Despite a trivial decline in the CE by less than 0.01 eV, in 1.4×10^{-2} *a.u.*, the CE remains stable by the EF, for all doped C_{20} , regardless of

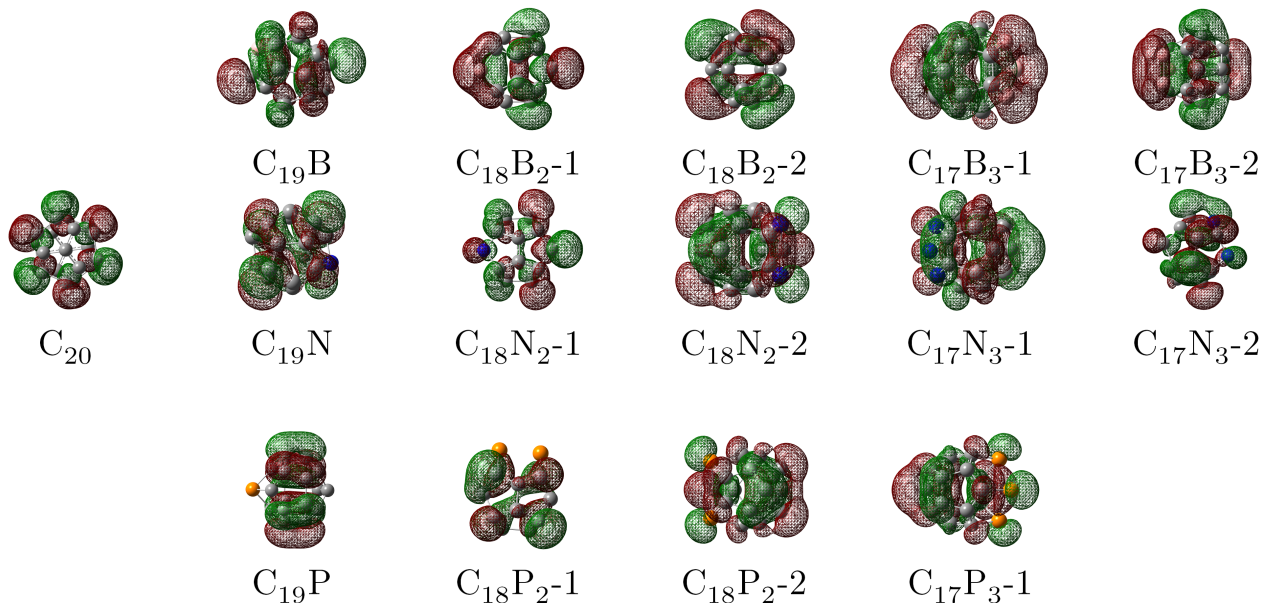


Figure 3: The HOMO plots for C_{20} and $C_{20-n}X_n$ ($n = 1, 2,$ and 3 ; $X = B, N,$ and P). The colors of the orbitals: red and green shows the positive and negative wave function, respectively. Atoms color code: pink, boron; blue, nitrogen; yellow, phosphorus; grey, carbon.

the type and number of doped atoms as well as the structures, which demonstrates, the CE is independent from EF, to the most extent (for more details see fig. S1). According to Fig. 2, the CE of all doped C_{20} are in favorable range, approximately from 7.45 to 7.8 eV, although they have slightly less CE Compared to C_{20} with around 7.87 eV, which can be due to the solid fullerene structure originating from double bonds among Carbon atoms ($C=C$) (or Hybrid structure) while in areas with the doped atoms, they are replaced by single bonds ($C-X$). The stability of $C_{19}B$ and $C_{19}N$ also have been computationally investigated and proven by calculating the binding and formation energy per atom in another literature.³¹

Fig. S1 depicts CE/EF ratio for each of doped C_{20} in more details. Apparently, CE adopted a downward trend as the number of the doped atoms increased, which could be resulted from fewer double bonds in the fullerene's structure. $C_{19}N$ and $C_{19}B$ with about 7.8 and 7.78 eV respectively, exhibited the closest CE to C_{20} , which could be labeled as the most stable structures among them. The CE of the doped fullerenes with the same number of doped atoms appears in almost the same range

such as $C_{18}N_2-1$ and 2 (~ 7.72 eV), $C_{17}N_3-1$ and 2 (~ 7.62 eV), $C_{18}B_2-1$ and 2 (~ 7.67 eV), and $C_{17}B_3-1$ and 2 (~ 7.47 eV), however with one exception; Compared to others, there is a gap between $C_{18}P_2-1$ and 2, by nearly 0.07 eV.

As presented by Fig. 3 and 4, which are the HOMO-LUMO plots of the doped C_{20} s, the electron density distribution of the HOMO-LUMO orbitals on the B and N atoms (in B and N-doped C_{20} s) are more than the P atoms (in the P-doped), explaining the B and N doped fullerenes can have better interaction against CO_2 .

The ESP map in figure 5 (color coded) depicts the charge distribution in the fullerenes. The areas with B atoms show small amount of electron density (bluer) while there is more negative charge focused on the areas with N atoms. Therefore, the B atoms are more susceptible to act as an electron acceptor and likely receive CO_2 π electrons to some extent, through the electron hole, more located on B. On the contrary, N atoms are more likely to play the role of an electron donor and donate their non-bonding electrons, which reside more on the N atoms, to CO_2 π^* orbitals throughout adsorption process. P atoms could display the both behavior.

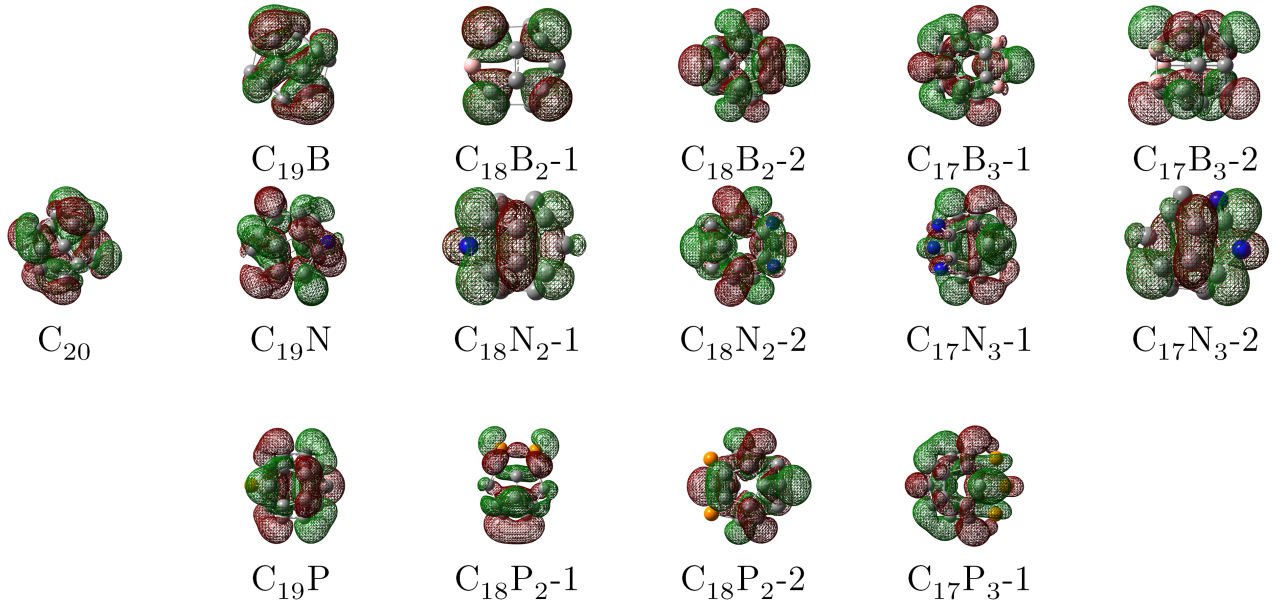


Figure 4: The LUMO plots for C_{20} and $C_{20-n}X_n$ ($n = 1, 2,$ and 3 ; $X = B, N,$ and P). The colors of the orbitals: red and green shows the positive and negative wave function, respectively. Atoms color code: pink, boron; blue, nitrogen; yellow, phosphorus; grey, carbon.

It must be noted that using the terms electron acceptor and donor are for clarifying the adsorption process and interactions certainly are not in the scale to be considered as reactions or strong interactions.

CO₂ adsorption in the presence and absence of electric field

To explore the effect of EF on CO₂ capturing over the X-doped fullerenes, an external EF was applied in perpendicular direction ($-z$ direction). Fig. 6 outlines AE (eV), AH (\AA), and CO₂ angle ($^\circ$) for X doped C_{20} in the range of 0 to $0.02 a.u.$ EF. Needless to mention, the larger AE represents stronger interaction between the doped fullerenes and CO₂. The AH could be taken into account as a parameter that confirms stronger interactions since, even by doping C_{20} , it is likely to observe physisorption rather than chemisorption in parts with doped atoms. The CO₂ angle values indicate that the CO₂ polarity changes when it is adsorbed by doped fullerene.

According to the Fig. 6, generally, there is a rise in the AE, in the most cases as well as C_{20} , by scanning the EF, implying that larger

EF contributes to CO₂ capture and the interaction between CO₂ and doped fullerenes can be strengthened by elevating EF. The B-doped fullerenes have the largest AE among all, along with a slight upward trend in the range of -0.53 to $-0.71 eV$, as the EF increases. To distinguish between physisorption and chemisorption, ΔG° and ΔH° of the adsorption process have to be considered. The magnitudes of ΔG° are between 0 and $-0.21 eV$ for physisorption and between -0.83 and $-4.15 eV$ for chemisorption while the amounts of ΔH° are from -0.022 to $-0.22 eV$ and from -0.83 to $-2.07 eV$, for physisorption and chemisorption, in order.³² The AH for B-doped C_{20} is almost the smallest in proportion to others, from approximately 1.33 to 1.43\AA as the EF rises, which approves the AE results. The CO₂ angle has changed dramatically (in the range of $120^\circ - 125^\circ$), which are less than the angle of O-C-O in the presence of C_{20} molecule, indicating a stronger interaction between the B-doped fullerenes and CO₂. Thus, it can be concluded that adsorption nature on B-doped fullerenes is physicochemical, resulting in a effective CO₂ adsorption process.

Apparently, after the B-doped fullerenes, the

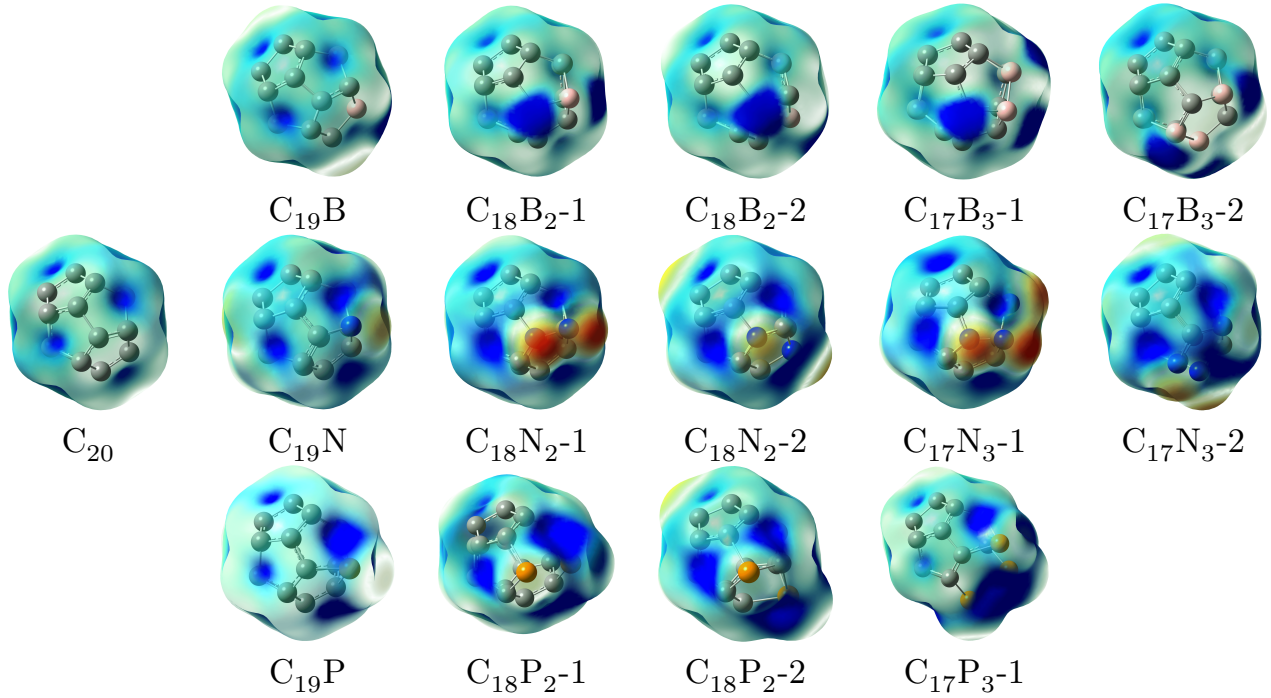


Figure 5: Electrostatic potential surface map for C_{20} and $C_{20-n}X_n$ ($n = 1, 2,$ and 3 ; $X = B, N,$ and P) with isovalue $0.004 \text{ e}\text{\AA}^{-3}$. The color range in the ESP maps varies from blue (more negative) to red (more positive). Atoms color code: pink, boron; blue, nitrogen; yellow, phosphorus; grey, carbon.

N-doped fullerenes also display a satisfactory activity against CO_2 compared to C_{20} . The AE for $C_{20-n}N_n$ lies in the area between -0.3 and -0.5 eV by EF, which exhibit, despite smaller AE in comparison with B-doped, the adsorption could be taken into account as physicochemical as well. Similar to B-doped, the AH of N-doped fullerenes appears in the range of 1.37 to 1.5 \AA , confirming the AE data. Although CO_2 angle for N containing C_{20} includes a wide area (117° - 128°), it certainly does not contradict the AE and AH findings. Evidently, the AE for the P-doped samples is in the same range as C_{20} , meaning that they have a similar performance to the C_{20} fullerene in the presence of electric field. Although the CO_2 angle for P-doped fullerenes alongside C_{20} is less than 130° , the range in which AEs appear in the absence of EF (between -0.20 and -0.28 eV) shows that physisorption plays the main role in the process. However, due to the positive impact of increasing EF on the AE, it grows to the area between nearly -0.30 and -0.38 eV , adding more chemical properties to the nature of the ad-

sorption and converting it from physisorption to physicochemical adsorption. These results are in a good agreement with HOMO-LUMO analysis (see figure 3 and 4). It can be seen that the HOMO or LUMO orbitals of the fullerenes, which have shown a higher AE, are more concentrated on the doped atoms and their adjacent C atoms, strengthening their interaction with CO_2 .

Fig. S2 illustrates a detailed line graph of AE (eV), AH (\AA), and CO_2 angle ($^\circ$) vs. EF. Except $C_{18}N_2-1$ and $C_{17}N_3-1$, the AE of Doped C_{20} grow or remain steady (after some fluctuations in a few cases), by scanning the EF, emphasizing that escalating EF has positive effect on AE. Despite some exceptions, C_{20} and most of the doped fullerenes have undergone a sudden growth in AE (by -0.05 eV), in approximately 0.018 a.u. , after a gradual increase or decrease. In some cases, we saw dramatic changes in the AH; For example the AH of $C_{17}P_3-1$, $C_{18}N_3-2$, $C_{17}B_3-1$ and $C_{17}B_3-2$ increased by nearly 0.07 \AA . On the other hand, $C_{19}N$, $C_{18}P_2-1$ and $C_{18}P_2-2$ decline with al-

most 0.06 Å.

Conclusion

In this study, DFT computations have been utilized to assess some B, N, and P doped fullerenes thermodynamic stability and prospect of B, N, and P addition into C_{20} structure along with their potential to capture CO_2 as well as the impact of electric field on this attribute. The cohesive energy was obtained to determine the doped fullerenes' stability. Although the cohesive energies of $C_{20-n}X_n$ were slightly smaller than C_{20} , they were all in a favorable range. There were nearly no changes in the cohesive energies, as electric field increased. The B and N doped fullerenes displayed a far better performance in adsorbing CO_2 with the adsorption energy in the range of -0.53 to -0.71 eV and -0.3 to -0.5 , respectively, in comparison with C_{20} , showing that adsorption process have gained chemical nature and become physicochemical adsorption. As a result of growing EF's effect on CO_2 adsorption, the AE of P-doped and C_{20} rise and interaction between CO_2 and samples obtains some chemical characteristic. Moreover, by the assistance of HOMO-LUMO plots, unlike P-doped fullerenes, we observed that the HOMO-LUMO orbitals were distributed largely on the B, N, and neighboring C atoms in B and N inserted C_{20} . The ESP map aided us to evaluate charge distribution on the fullerenes' surface and hypothesize about the mechanism of adsorption.

Lastly, the present study illuminates the B, N, and P doped fullerenes potential as a CO_2 adsorbent. B and N containing fullerenes show a splendid activity against CO_2 as a promising adsorbent and using them can be considered an efficient way for CO_2 capture in absence and presence of electric field.

Acknowledgement The authors acknowledge the UNESCO UNISA iThemba-LABS/NRF Africa Chair in Nanoscience & Nanotechnology (U2ACN2) and the Centre for High-Performance Computing (CHPC), South Africa for providing computational resources and facilities for this research project.

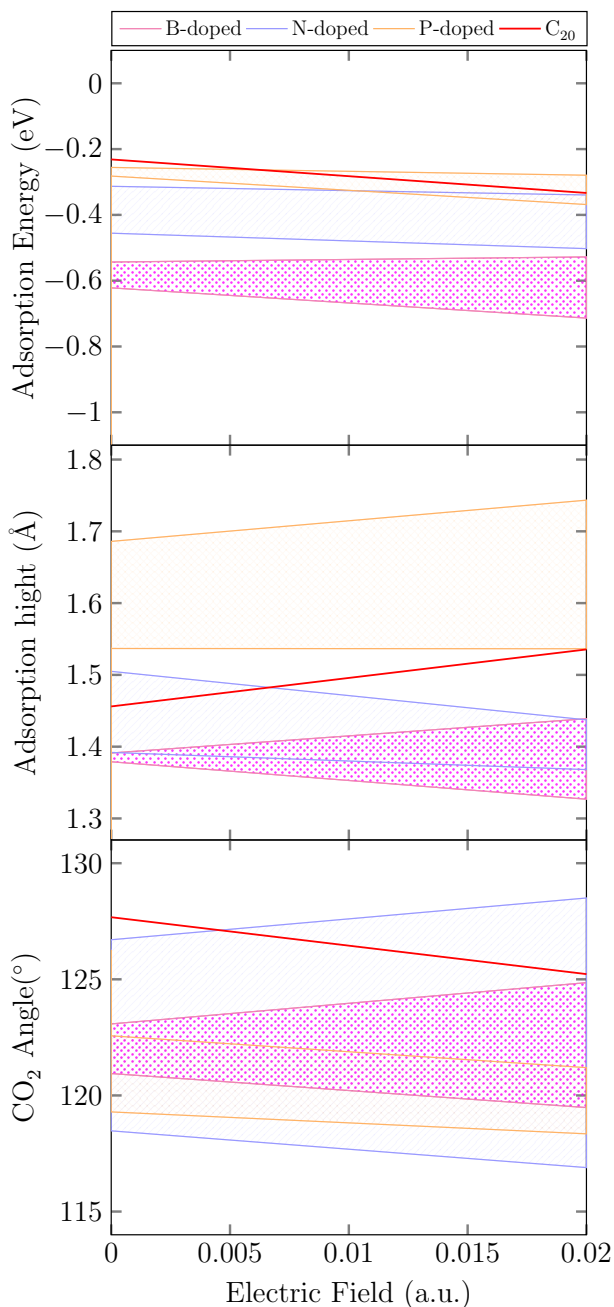


Figure 6: Variation of (a) adsorption energy (eV) (b) adsorption height (Å) (c) C_{20} angle ($^{\circ}$) for C_{20} , B, N, and P-doped C_{20} in 0–0.02 a.u. electric field.

Supporting Information Available

Figures of variation of cohesive energy, adsorption energy, adsorption height, and CO₂ angle are presented in supporting information.

References

- (1) Internationale Energieagentur, Ed. *World energy outlook 2011*; World Energy Outlook 2011; 2011
- (2) Kheshgi, H.; De Coninck, H.; Kessels, J. Carbon dioxide capture and storage: Seven years after the IPCC special report. *Mitigation and Adaptation Strategies for Global Change* **2012**, *17*, 563–567
- (3) Lee, K. B.; Sircar, S. Removal and recovery of compressed CO₂ from flue gas by a novel thermal swing chemisorption process. *AIChE Journal* **2008**, *54*, 2293–2302
- (4) Jiao, Y.; Du, A.; Zhu, Z.; Rudolph, V.; Smith, S. C. A density functional theory study of CO₂ and N₂ adsorption on aluminium nitride single walled nanotubes. *Journal of Materials Chemistry* **2010**, *20*, 10426
- (5) Jiao, Y.; Du, A.; Zhu, Z.; Rudolph, V.; Smith, S. C. Adsorption of Carbon Dioxide and Nitrogen on Single-Layer Aluminum Nitride Nanostructures Studied by Density Functional Theory. *The Journal of Physical Chemistry C* **2010**, *114*, 7846–7849
- (6) Sun, Q.; Wang, M.; Li, Z.; Du, A.; Searles, D. J. Carbon Dioxide Capture and Gas Separation on B₈₀ Fullerene. *The Journal of Physical Chemistry C* **2014**, *118*, 2170–2177
- (7) Lee, H.; Li, J.; Zhou, G.; Duan, W.; Kim, G.; Ihm, J. Room-temperature dissociative hydrogen chemisorption on boron-doped fullerenes. *Physical Review B* **2008**, *77*, 235101
- (8) Sun, Q.; Li, Z.; Searles, D. J.; Chen, Y.; Lu, G. M.; Du, A. Charge-Controlled Switchable CO₂ Capture on Boron Nitride Nanomaterials. *Journal of the American Chemical Society* **2013**, *135*, 8246–8253
- (9) Rezaee, P.; Naeij, H. R. A new approach to separate hydrogen from carbon dioxide using graphdiyne-like membrane. *Scientific Reports* **2020**, *10*, 13549
- (10) Rezaee, P.; Naeij, H. R. Graphenylene-1 membrane: An excellent candidate for hydrogen purification and helium separation. *Carbon* **2020**, *157*, 779–787
- (11) Agrawal, P. S.; Belkhole, P. N.; Brijjuriya, D. S.; Gouda, S. P.; Rokhum, S. L. Stimulation in fullerene for adsorbing pollutant gases: A review. *Chemical Physics Impact* **2023**, *6*, 100156
- (12) Gao, B.; Zhao, J.-x.; Cai, Q.-h.; Wang, X.-g.; Wang, X.-z. Doping of Calcium in C₆₀ Fullerene for Enhancing CO₂ Capture and N₂O Transformation: A Theoretical Study. *The Journal of Physical Chemistry A* **2011**, *115*, 9969–9976
- (13) Huang, W.; Shi, M.; Song, H.; Wu, Q.; Huang, X.; Bi, L.; Yang, Z.; Wang, Y. Hydrogen storage on chains-terminated fullerene C₂₀ with density functional theory. *Chemical Physics Letters* **2020**, *758*, 137940
- (14) Babarao, R.; Eddaoudi, M.; Jiang, J. W. Highly Porous Ionic rht Metal-Organic Framework for H₂ and CO₂ Storage and Separation: A Molecular Simulation Study. *Langmuir* **2010**, *26*, 11196–11203
- (15) Nandi, S.; De Luna, P.; Daff, T. D.; Rother, J.; Liu, M.; Buchanan, W.; Hawari, A. I.; Woo, T. K.; Vaidhyanathan, R. A single-ligand ultramicroporous MOF for precombustion CO₂ capture and hydrogen purification. *Science Advances* **2015**, *1*, e1500421

- (16) Li, L.; Duan, Y.; Liao, S.; Ke, Q.; Qiao, Z.; Wei, Y. Adsorption and separation of propane/propylene on various ZIF-8 polymorphs: Insights from GCMC simulations and the ideal adsorbed solution theory (IAST). *Chemical Engineering Journal* **2020**, *386*, 123945
- (17) Li, Y.; Liang, F.; Bux, H.; Yang, W.; Caro, J. Zeolitic imidazolate framework ZIF-7 based molecular sieve membrane for hydrogen separation. *Journal of Membrane Science* **2010**, *354*, 48–54
- (18) Hug, S.; Stegbauer, L.; Oh, H.; Hirscher, M.; Lotsch, B. V. Nitrogen-Rich Covalent Triazine Frameworks as High-Performance Platforms for Selective Carbon Capture and Storage. *Chemistry of Materials* **2015**, *27*, 8001–8010
- (19) He, L. et al. A nitrogen-rich covalent organic framework for simultaneous dynamic capture of iodine and methyl iodide. *Chem* **2021**, *7*, 699–714
- (20) Walczak, R.; Savateev, A.; Heske, J.; Tarakina, N. V.; Sahoo, S.; Epping, J. D.; Kühne, T. D.; Kurpil, B.; Antonietti, M.; Oschatz, M. Controlling the strength of interaction between carbon dioxide and nitrogen-rich carbon materials by molecular design. *Sustainable Energy & Fuels* **2019**, *3*, 2819–2827
- (21) Kutorglo, E. M.; Hassouna, F.; Beltzung, A.; Kopecký, D.; Sedlářová, I.; Šoóš, M. Nitrogen-rich hierarchically porous polyaniline-based adsorbents for carbon dioxide (CO₂) capture. *Chemical Engineering Journal* **2019**, *360*, 1199–1212
- (22) Kang, K. Y.; Lee, B. I.; Lee, J. S. Hydrogen adsorption on nitrogen-doped carbon xerogels. *Carbon* **2009**, *47*, 1171–1180
- (23) Giraudet, S.; Zhu, Z.; Yao, X.; Lu, G. Ordered Mesoporous Carbons Enriched with Nitrogen: Application to Hydrogen Storage. *The Journal of Physical Chemistry C* **2010**, *114*, 8639–8645
- (24) Li, L.; Zhang, T.; Duan, Y.; Wei, Y.; Dong, C.; Ding, L.; Qiao, Z.; Wang, H. Selective gas diffusion in two-dimensional MXene lamellar membranes: insights from molecular dynamics simulations. *Journal of Materials Chemistry A* **2018**, *6*, 11734–11742
- (25) Khan, A. A.; Ahmad, R.; Ahmad, I.; Su, X. Selective adsorption of CO₂ from gas mixture by P-decorated C₂₄N₂₄ fullerene assisted by an electric field: A DFT approach. *Journal of Molecular Graphics and Modelling* **2021**, *103*, 107806
- (26) Khan, A. A.; Ahmad, R.; Ahmad, I. Removal of nitrous and carbon mono oxide from flue gases by Si-coordinated nitrogen doped C₆₀-fullerene: A DFT approach. *Molecular Catalysis* **2021**, *509*, 111674
- (27) Esrafil, M. D. Electric field assisted activation of CO₂ over P-doped graphene: A DFT study. *Journal of Molecular Graphics and Modelling* **2019**, *90*, 192–198
- (28) Wang, Y.; Yang, Z.; Zhang, N.; Wang, D.; Wang, R.; Peng, W.; Zhang, J.; Liu, J.; Zhang, J. CO₂ capture and separation with metalloporphyrin nanosheets in an electric field: A DFT study. *Applied Surface Science* **2023**, *610*, 155340
- (29) Wang, Y.; Wang, H.; Zhang, N.; Wang, D.; Wang, R.; Peng, W.; Zhang, J.; Liu, J.; Zhang, J. CO₂ Capture and Separation by Mono-Vacancy Doped Graphene in Electric Field: A DFT study. *Chemistry-Select* **2023**, *8*, e202203408
- (30) Sathishkumar, N.; Wu, S.-Y.; Chen, H.-T. Charge-regulated, electric-field and combined effect controlled switchable CO₂ capture and separation on penta-C₂N nanosheet: A computational study. *Chemical Engineering Journal* **2021**, *407*, 127194
- (31) Hassani, N. C₂₀ fullerene and its boron- and nitrogen-doped counterparts as an efficient catalyst for CO oxidation. *Molecular Physics* **2020**, *118*, e1766708

- (32) Liu, Q.-S.; Zheng, T.; Wang, P.; Jiang, J.-P.; Li, N. Adsorption isotherm, kinetic and mechanism studies of some substituted phenols on activated carbon fibers. *Chemical Engineering Journal* **2010**, *157*, 348–356